Hindawi
Journal of Nanomaterials
Volume 2019, Article ID 1310792, 16 pages
https://doi.org/10.1155/2019/1310792

Review Article

Recent Progress on Mg- and Zn-Based Alloys for Biodegradable Vascular Stent Applications

Ying Liu[1,2], **Bingheng Lu**[1] and **Zhixiong Cai**[3,4]

[1]*State Key Laboratory for Manufacturing System Engineering, School of Mechanical Engineering, Xi'an Jiaotong University, Xi'an 710049, China*
[2]*The Key Laboratory of Biomedical Information Engineering of Education Ministry, The Department of Biomedical Engineering, Xi'an Jiaotong University, Xi'an 710049, China*
[3]*Key Laboratory of Biomedical Information Engineering of Ministry of Education, Institute of Biomedical Analytical Technology and Instrumentation, School of Life Science and Technology, Xi'an Jiaotong University, Xi'an 710049, China*
[4]*Mengchao Med-X Center, Fuzhou University, Fuzhou 350116, China*

Correspondence should be addressed to Zhixiong Cai; caizhixiong1985@163.com

Received 10 June 2019; Revised 5 September 2019; Accepted 30 September 2019; Published 5 November 2019

Academic Editor: Giuseppe Compagnini

Copyright © 2019 Ying Liu et al. This is an open access article distributed under the Creative Commons Attribution License, which permits unrestricted use, distribution, and reproduction in any medium, provided the original work is properly cited.

Currently, biodegradable metals for implantation applications are widely investigated to replace biodegradable polymeric implantations, which may cause inflammatory or adverse local tissue reactions. Amongst these metals, magnesium (Mg) and zinc (Zn) alloys with good biocompatibility, mechanical properties, and corrosion resistance are being widely investigated. In this review, the criteria for biodegradable vascular stents, and the advantages and limitations of biodegradable Mg and Zn vascular stents, are summarized and evaluated. By summarizing and discussing recent research on Mg- and Zn-based alloys used as biodegradable vascular stents, this review considered many alloys that can potentially serve as biodegradable vascular stents and suggests future research directions for the development of Mg- and Zn-based alloys as biodegradable metal stents.

1. Introduction

Vascular stents are being widely used to restore and maintain the blood flow in diseased vessels and treat coronary artery diseases, such as thrombus and atherosclerosis, which are pernicious to blood flow continuity. Permanent bare metal stents (BMS) that can mainly provide mechanical support and drug-eluting stents (DES) that can provide additional drug release therapy are being used [1, 2]. Both BMS and DES can induce platelet adhesion, activation, and thrombus formation, but DES does not improve the performance of late-stage thrombosis. The cytotoxic drugs used in DES are designed to reduce the smooth muscle cell growth and can inhibit reendothelialization [3, 4]. In this situation, biodegradable or bioabsorbable vascular stents (BVS) are used to provide effective mechanical support for artery walls as vessel scaffolding and are subsequently metabolized by the human body, which is an effective way to decrease the incidence of late and very late thrombosis. Thus, these stents are considered to be ideal for minimizing the long-term harm caused by permanent stents [5].

Metallic- and polymer-based BVS have distinct material properties and performance, including expansion properties, elastic and time-dependent recoil properties, radial strength, and degradation products. Metallic BVS exhibit rapid and full expansion and stable and acute mechanics. Moreover, time-dependent properties are typical for polymer BVS with underexpansion and can lead to late-stage thrombosis. The heterogeneous structure of polymers eventually causes structural collapse. The outer layers of polymer stents have a smooth crystalline structure made of highly aligned polymers, while the inner core has a much less ordered structure. When the polymer stents inflate, these regions are disrupted, which leads to the early loss of integrity in parts of the

structure. In contrast, metallic stents can more easily acquire a uniform microstructure to provide stable acute mechanics and improve the corrosion behavior. Otherwise, polymer stents may cause inflammation in the coronary artery, which may lead to a prothrombotic environment. According to Bangalore et al., cobalt chromium everolimus eluting stents are safer than bare metal stents in terms of thrombosis, death, and myocardial infarction risk and significantly reduce the stent thrombosis rate and risk of death after one year compared with biodegradable polymer drug-eluting stents [6]. Moreover, the BVS material, design, fabrication, and corrosion behavior *in vitro* and *in vivo* are crucial considerations for metallic stents. Therefore, this review focuses on the materials, stent design, fabrication, and corrosion behavior of metallic BVS.

First-generation stent metals mainly include Co-Cr, Ni-Ti alloys, and stainless steel, which are permanently implanted. First-generation materials have been applied in the biomaterial field owing to their high mechanical properties, good corrosion resistance, and low cost [6, 7]. However, they are gradually replaced by second-generation materials owing to cracks caused by fatigue corrosion and the side effects of the Co and Ni elements [8].

DES can prevent inflammation and maintain blood flow continuity. However, cytotoxic drugs can also inhibit reendothelialization, induce platelet adhesion, and cause the activation and formation of thrombus. Additionally, DES does not have better performance with regard to late-stage thrombosis compared with bare metal stents. Thus, there is motivation for developing next-generation materials for vascular stents, such as BVS with a drug-eluting function [9].

As next-generation biomaterials, biodegradable or bioabsorbable magnesium (Mg) and zinc (Zn) alloys are being considered for temporary medical support device placement applications. Mg and Zn alloys have the greatest potential for use as stents that can retain their mechanical properties and provide temporary support to the blood vessel for approximately six months, after which they are broken down, metabolized, and excreted by the human body to restore the native vasomotion and eliminate sources of inflammation or thrombosis [10, 11].

Mg alloys with good biocompatibility, nontoxic degradation products, and relatively high mechanical properties can satisfy the BVS requirements. Additionally, Mg is one of the two metals that have been investigated in several animal and clinical studies [12]. However, the relatively high rate of degradation (within 60-90 days) and associated evolution of hydrogen are severe problems and require further improvement [13]. Zn alloys can degrade at a rate of approximately 0.02 mm/year, which satisfies the BVS requirements in terms of providing support to blood vessels for a reasonable period. However, their relatively poor mechanical properties remain a critical problem that must be addressed [14, 15].

BVS materials must achieve rigorous biocompatibility, a reasonable degradation rate, and good mechanical properties, simultaneously. This review focused on next-generation nonferrous biomaterials, namely, Mg and Zn alloys. Recent studies on Mg and Zn alloys used as BVS and various relevant perspectives are discussed in this paper.

2. Criteria for Biodegradable Vascular Stents

Many extreme conditions have to be satisfied by BVS and are mainly divided into three groups: mechanical properties, degradation, and biocompatibility (Table 1) [16]. The BVS material must be fully biocompatible without any degradation by-products *in vivo*, and the degradation must occur at a reasonable rate for long-term benefits.

2.1. Mechanical Properties. Some crucial stent characteristics are required for better clinical results, including low crossing profile, high flexibility, high biocompatibility, high radial strength, low metallic surface area, good trackability, and easy deployment. For metallic stents, there are three main aspects that require attention: stent construction, stent geometry, and stent strut thickness.

The structure of metallic stents can be divided into three components: the coil, tubular mesh, and tubular with two specification types, namely, the slotted tube and modular tube. The coil stents are characterized by metallic wires or strips formed into a circular coil shape. Tubular mesh stents are characterized by wires wound in a meshwork forming a tube stent. Slotted tube stents consist of metal tubes from which a stent design is laser-cut. Amongst the three structural groups, the slotted tube design exhibits greater radial strength and produces superior clinical results compared with the more flexible mesh and coil structure stents. Moreover, the modular stent design can also offer a balance between coil flexibility and the radial strength of slotted tube design.

The stent geometry is another important influencing factor for restenosis. The increasing number of strut-strut intersections leads to a proportional increase in the neointimal area, and the reduced number of the intersections causes the reduction of vascular injuries. Thus, stents tend to be designed with less struts to obtain better clinical results with regard to the occurrence of restenosis.

The stent strut thickness is a key factor in stent design and can be divided into four levels: ultrathin (60-80 μm), thin (81-100 μm), intermediate (101-120 μm), and thick (>120 μm). For metallic stents, thinner struts have greater deliverability, while thinner struts are associated with lower restenosis rates. Although the immediate performance including radiovisibility, radial strength, and arterial wall support can be improved by increasing the strut thickness, excessive strut thickness causes more vascular injuries, triggers more intimal hyperplasia, and entails higher risk of restenosis compared with thinner struts. To satisfy the scaffolding function and maintain an adequate radiovisibility and radial strength with a thinner strut thickness, a novel process and metallic materials with high mechanical properties are required.

To achieve reasonable scaffolding, it is recommended that the mechanical properties are close to those of 316L stainless steel, which is the standard vascular stent material. The mechanical properties required for stents include the yield strength (YS), ultimate tensile strength (UTS), elastic modulus or Young's modulus (YM), and elongation. These mechanical material properties indicate the radial strength, acute and chronic recoil, axial and radial

Table 1: Criteria for biodegradable vascular stents.

Properties		Constraints
Mechanical properties [16, 17]	Yield strength	>200 MPa
	Ultimate tensile strength	>300 MPa
	Elongation	>15-18%
	Ratio of yield strength to elastic modulus	>0.16
	Elastic recoil on expansion	<4%
	Resistance to cyclic fatigue	>10-20 million cycles before failure
Degradation	Degradation period	Mechanical integrity: 3-6 months Full absorption: 12-24 months [18]
	Degradation rate	Penetration rate < 0.02 mm/year [16, 17, 19]
Biocompatibility	Biocompatibility	Nontoxic, noninflammatory, and no allergenic potential [16, 17]

flexibility, deliverability, profile, and lifetime integrity [18]. Materials with high UTS and relatively low YS are recommended for vascular stents. A low YS is desirable for a balloon expanding at low pressure, and a high YS with a relatively large elastic deformation can lead to acute recoil during or after balloon expansion [20]. Typically, however, materials have high YS and high UTS, but there are still no criteria for BVS resistance to cyclic fatigue. The lifetime of 316L stainless steel permanent stents is more than 400 million cycles in 10 years. According to the degradation criteria, biodegradable stents must retain their mechanical properties for three to six months and 10-20 million cycles before failure satisfies the BVS requirements [10, 21].

The mechanical properties of Mg alloys are much weaker compared with 316L SS. Thus, many processing methods, such as alloying and deformation, have been employed to improve them. Zn, Al, Y, Nd, Ca, Zr, and rare earth elements are the main alloying elements for forming strengthening phases to further increase the mechanical properties. Many novel processing techniques are also employed to improve the mechanical properties, including cold deformation methods such as cold drawing, extrusion, and severe plastic deformation (SPD). Mg alloys are close-packed hexagonal (HCP) structures with only three slip systems, which make deformation substantially more difficult compared with face-centered cubic (FCC) and body-centered cubic (BCC) structures with 12 slip systems at room temperature. However, once Mg alloys deform, their mechanical properties are significantly improved. In research and practical applications, alloying is always combined with deformation to improve the mechanical properties of Mg alloys.

Zn and its alloys exhibit even more inferior mechanical properties compared with Mg alloys, and this is the biggest limitation for their application as stents. Additionally, Zn is an HCP structure and thus difficult to deform. Alloying is a very effective approach toward improving the mechanical properties. With regard to the alloying elements, the effect on the degradation rate, biocompatibility, and corrosion homogeneity should also be considered. In research, alloying is occasionally combined with extrusion to improve the mechanical properties of Zn alloys.

2.2. Degradation and Biocompatibility. For the use of Mg and Zn alloys as vascular stents, the degradation rate, degradation products, and biocompatibility are crucial considerations. Additionally, the biocompatibility is determined by the solubility and degradation products. Essentially, the corrosion rate of the BVS material should be less than 0.02 mm per year to satisfy the lifetime and degradation requirements of stents and avoid the excess concentration of degradation products that can cause long-term symptoms [19].

Mg alloys have a relatively high degradation rate, which can lead to degradation in the body within one to three months. Thus, coating that includes MgF_2 film, poly(lactic-co-glycolic acid) (PLGA), poly(carbonate urethane) urea (PCUU), and poly(ester urethane) urea (PEUU) is an effective approach toward decreasing the degradation rate. The Mg element itself is essential to human metabolism with a relatively high toleration level of 121 mg/L in blood. When alloyed with other elements, the biocompatibility and amount should also be considered.

Pure Zn exhibits a better degradation rate compared with Mg and iron-based stents. Research results have revealed that the degradation rate and products of Zn are less than 50 μm/year in six months and less than those of Zn carbonate and Zn oxide, respectively. Moreover, Zn is also an essential element in parts of the human body, such as the muscles, bones, skin, and liver. The recommended daily dose of Zn for adults is 6.5 to 15 mg/day [22]. Because a Zn-based stent can comprise approximately 50 mg of pure Zn, which degrades within 6 to 12 months, the Zn content is not sufficiently excessive to cause harm to the human body [23]. Considering that there are no animal experiment results indicating toxicity to cells and tissues, it is considered that the biocompatibility of Zn and its alloys can meet the BVS requirements.

3. Mg Alloys for Biodegradable Vascular Stents

3.1. Fabrication and Mechanical Properties of Mg Vascular Stents. Many advanced manufacturing methods have been employed for final stent fabrication, including electroforming, photochemical etching, laser cutting, and microelectromachining. There are two main technical processes for fabricating stents, including Mg foil and Mg microtube intermediates, as shown in Figures 1(a) and 1(b), respectively. In both processes, the as-cast Mg alloys are deformed to manufacture the billet and increase the mechanical properties. The

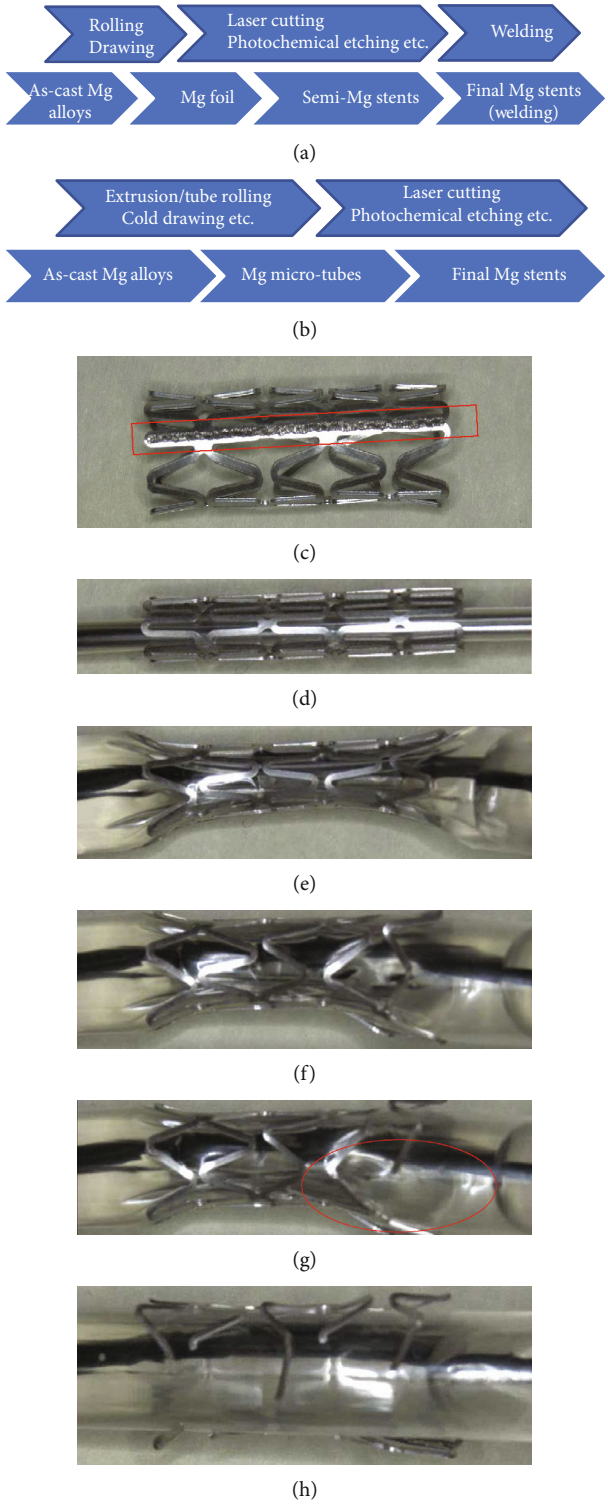

Figure 1: Two main technical processes of fabricating Mg stents: (a) Mg foil and (b) Mg microtube. (c) Photochemically etched AZ31 Mg stents with welding bar; failure of balloon expansion of welded Mg stent (d) before expansion; (e) dog bone period; (f) full expansion of two heads; (g) break of one stunt; (h) break of stent.

additional process of welding for Process A may lead to higher cost and a welding bar, which can result to nonuniform scaffolding stress and expansion failure (Figure 1(c), based on the author's work). The failure of balloon expansion for wielded stents is shown in Figure 1(c). During the balloon expansion, the stent (Figure 1(d)) succeeded in generating the "dog bone" shape (Figures 1(e) and 1(f)). Then, the strut of the right head broke (Figure 1(g)), and this resulted in complete stent failure (Figure 1(h)) owing to the nonuniform stress. Microtube billet fabrication has become the main fabrication process of Mg stents owing to its relatively low cost, short processing cycle, and better structure.

3.2. Processes and Mechanical Properties of Mg Microtubes

3.2.1. Concepts. In Mg microtube manufacturing, many advanced processes are employed, including direct and indirect extrusion, cold drawing, dieless drawing, and SPD.

Extrusion is the most important process for Mg alloys and includes direct extrusion, indirect extrusion, and lateral extrusion at an elevated temperature or room temperature. Elevated temperature extrusion is mostly applied because of the difficulty of deformation owing to the HCP structure. Dynamic recrystallization is expected to generate an isometric crystal microstructure for higher mechanical properties and better corrosion behavior. Extrusion at a relatively lower temperature can better improve the mechanical properties owing to the increase of sliding blocks.

Cold drawing is the most important method of fabricating bars, wires, tubes, and even metal sheets. Additionally, cold drawing is typically applied on stainless steels and copper alloys, which exhibit remarkable ductility and mechanical properties. The high deformation force, low tensile properties, and ductility of Mg alloys can cause the failure of cold drawing but are still effective in manufacturing Mg microtubes.

Dieless drawing is based on the drawing process but is better for large reduction compared with regular drawing. The large reduction is generated by pulling the tube and applying different temperatures along the tube using a moving heater and cooler.

Equal channel angular extrusion (ECAE) is an SPD method that can dramatically refine the microstructure and thereby improve the mechanical properties according to the Hall-Petch relationship.

Cyclic expansion extrusion (CEE) is another SPD method for achieving an ultrafine grain size and better mechanical properties.

3.2.2. Recent Studies on Processing and Mechanical Properties of Mg Microtubes. Although the deformation of Mg alloys is fairly difficult, it is still a low-cost, effective, and commonly used method of fabricating Mg microtubes and improving the mechanical properties such that they satisfy the vascular stent requirements. Moreover, this method has attracted a great deal of attention worldwide.

Mg-Nd-Zn-Zr (JDBM), AZ31, and WE43 microtubes were investigated by Liu et al. through a combination of hot extrusion (HE), direct/indirect extrusion (DE/IDE), cold rolling (CR), and drawing (CD) [24]. BVS microtubes made of three alloys were fabricated with an outer diameter of 3 mm and thickness of 180 μm (Figures 2(a)–2(d)). The

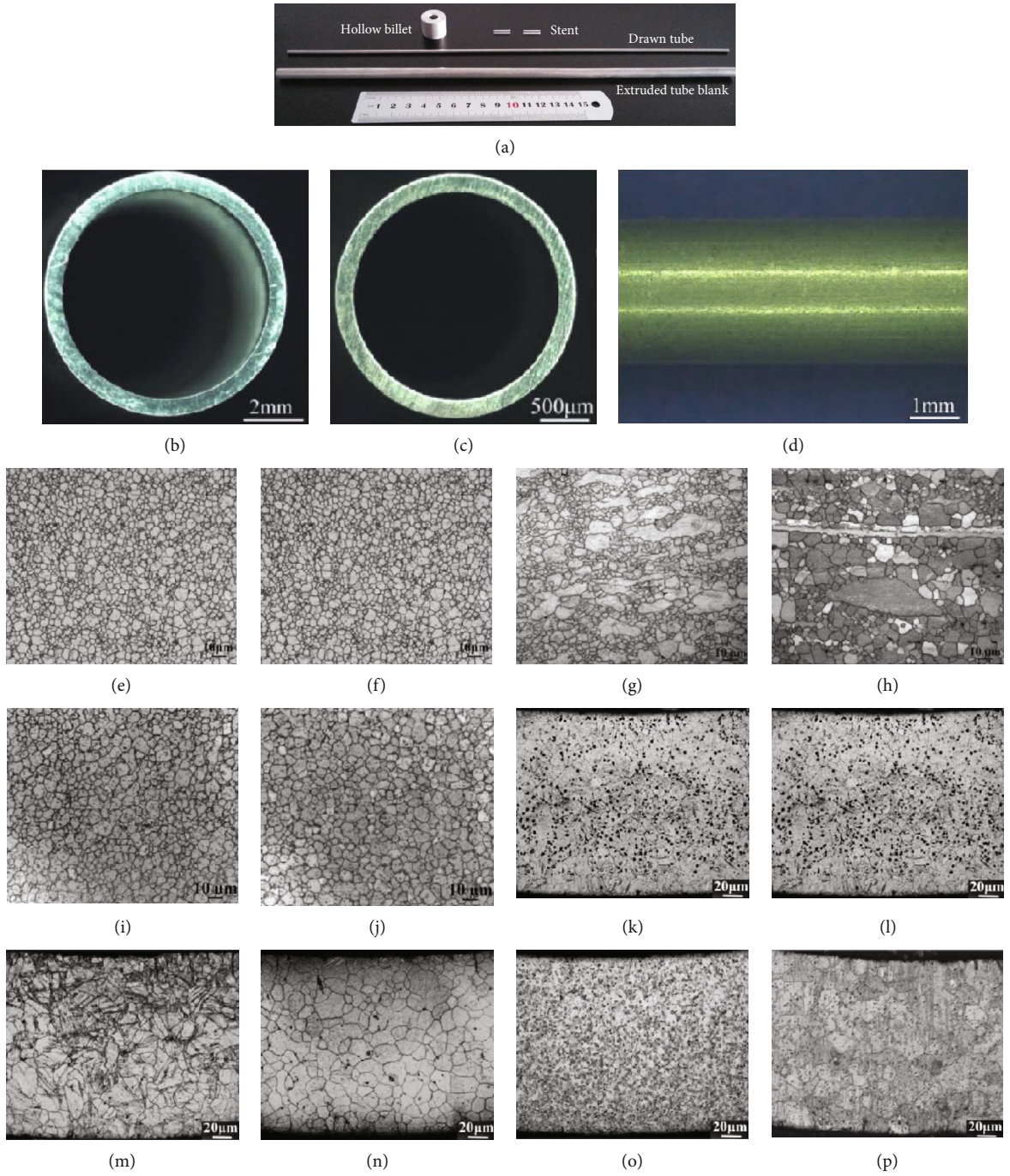

Figure 2: JDBM, AZ31, and WE43 microtubes with outer diameter of 3 mm and thickness of 180 μm [24]: (a) from hollow billet to stent; (b) cross-section of extruded blanks; (c) cold drawn tubes; (d) side surface of cold drawn tube. Microstructure of JDBM, AZ31, and WE43 extruded blanks: JDBM (e) cross-section and (f) longitudinal section; AZ31 (g) cross-section and (h) longitudinal section; WE43 (i) cross-section and (j) longitudinal section. Microstructure of cold drawn and annealed alloys: JDBM, (k) cold drawn and (l) annealed at 450°C for 1 h; AZ31, (m) cold drawn and (n) annealed at 450°C for 1 h; WE43, (o) cold drawn and (p) annealed at 450°C for 1 h.

extruded tube blanks (Figure 2(b)) and cold drawn tubes (Figure 2(c)) exhibited remarkable shape and thickness uniformity. The processing method could overcome the shortcoming of poor workability and allowed the fabrication of long tubes with a dimension error of 2.8%.

The microstructure of the JDBM, AZ31, and WE43 alloy extruded blanks is shown in Figures 2(e)–2(j). JDBM exhibited a complete recrystallized microstructure with an average grain size of 3.6 μm (Figures 2(e) and 2(f)), while the AZ31 alloys exhibited a noncomplete recrystallized microstructure with various coarse grains surrounded by fine recrystallized grains (Figures 2(g) and 2(h)). Additionally, the WE43 alloys exhibited a complete recrystallized microstructure with a slightly larger average size of 4.6 μm (Figures 2(i) and 2(j)). The microstructures of the three alloys, which were cold drawn and annealed at 450°C for 1 h, are shown in

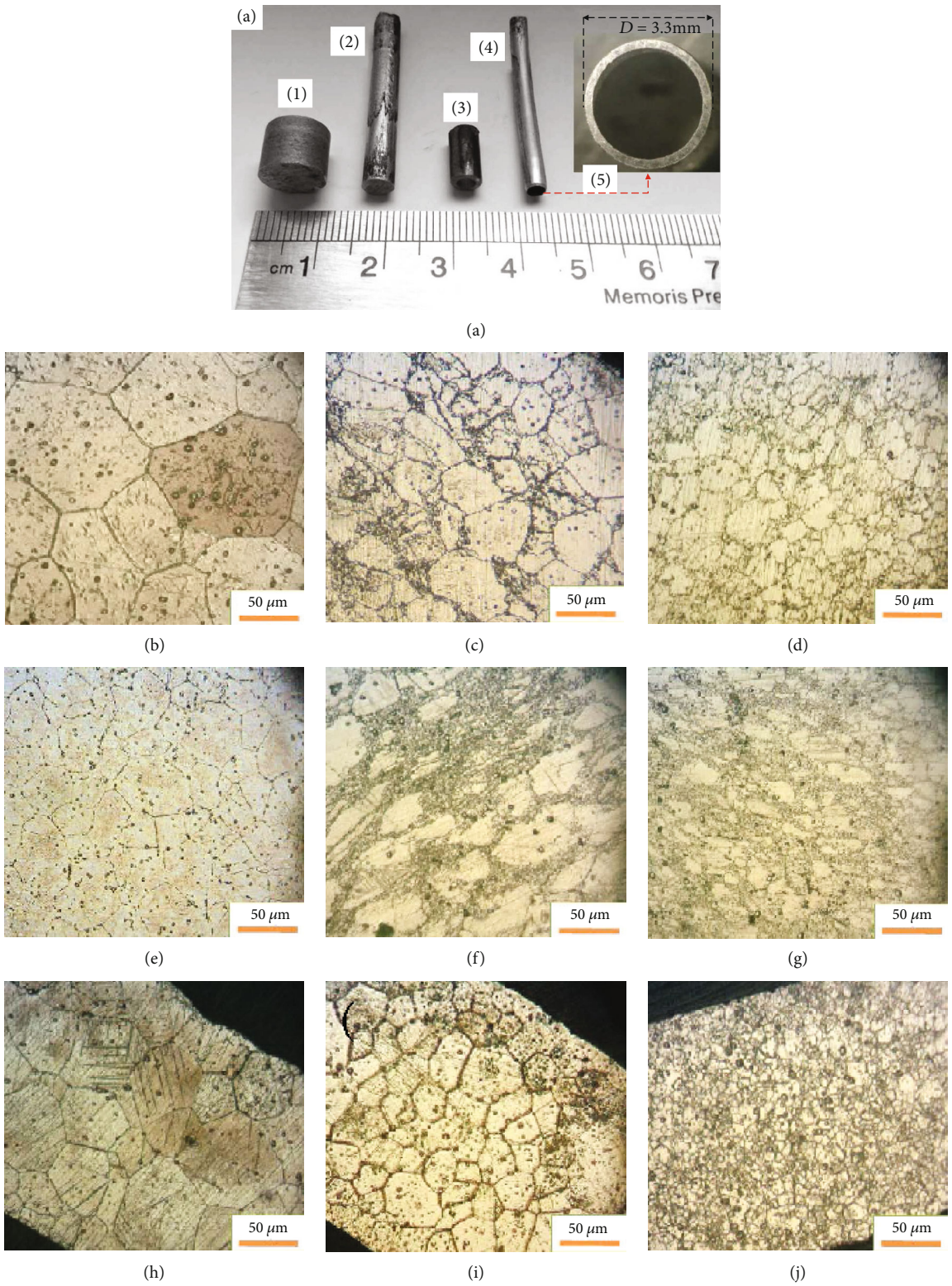

Figure 3: (a) Tube morphologies obtained by different processes: (1) CEE; (2) DE; (3) drilling; (4) MTE; (5) cross-section of final microtube. Microstructures of WE43 alloys: (b) as-received; (c) 1P CEE; (d) 2P CEE; (e) 0P+DE; (f) 1P+DE; (g) 2P+DE; (h) 0P+DE+MTE; (i) 1P+DE +MTE; (j) 2P+DE+MTE [25].

Figures 2(k)–2(p). After being cold drawn, all microstructures greatly deformed with a great amount of second phases and twins, which is an effective way for Mg alloys to achieve large deformation when slipping is inhibited. After being annealed, dynamic recrystallization (DRX) occurred and made the microstructure more uniform with an average

Table 2: Fabrication processes and properties of novel Mg microtubes.

Alloys	Process	YS (MPa)	UTS (MPa)	EL (%)	HV	Outer diameter (mm)	Thickness (mm)	Microstructure and average grain size
AZ31	DE+CD+CD [24]	172	—	16	—	3	0.18	DRX; 12.9 μm
	Dieless drawing [26]	—	—	—	—	3.35	0.69	—
JDBM	DE+CD+CD [24]	123	—	26	—	3	0.18	DRX; 10.9 μm
	Double extrusion [27]	220	267	48.8		3.5	0.25	—
WE43	DE+CD+CD [24]	113	—	10	—	3	0.18	DRX; 15 μm
	CEE+DE+MTE [25]	—	410	18.5	114	3.3	0.22	DRX; 5.5 μm
	CEE [28]	—	440 at highest	21 at highest	114 at highest	—	—	DRX+unrecrystallized grains
	ECAE+DE+MTE [29]		340	20	102	3.3	0.22	DRX; 3.5 μm
Mg-Zn-Y-Nd	DE+CD+annealing [19]	196	298	20		2	0.15	DR; 4.4 μm
ZM21	DE+drilling+HIDE+CD [30]	—	—	—	—	2.9	0.2	DRX+unrecrystallized grains
	DE+drilling+IDE+CD [31]	—	—	—	—	2.9	0.217	Inhomogeneous fine grains and twins
	DE+ECAE [32]	340	353	11.5	—	2.4	0.4	Fine grain; 2 μm
Mg-4Zn-1Y	HDE+annealing	240	330	20.4	—	—	—	DRX; 20 μm

grain size of 10.9 μm, 12.9 μm, and 15.0 μm, respectively. The mechanical properties were greatly determined by the microstructure and yield strength of the as-annealed JBDM, AZ31, and WE43 alloys and were 123 MPa, 172 MPa, and 113 MPa, while the elongations were 26%, 16%, and 10%, respectively.

Amani et al. fabricated a WE43 microtube using a new combined method based on the CEE, DE, and microtube extrusion (MTE); the morphologies obtained with each process are shown in Figure 3(a). The microstructures of the initial, first, and second passes of the CEE combined with DE and MTE are shown in Figures 3(b)–3(j). As can be seen in Figures 3(b)–3(d), the microstructure was refined using CEE, but the extent of refinement was limited. By combining CEE with DE, partial DRX occurred and became more complete with the increase of CEE passes (Figures 3(e)–3(g)). By combining CEE, DE, and MTE, complete DRX with an ultrafine isometric microstructure (average grain size of 5.5 μm) occurred and led to the increase of UTS, elongation, and hardness to 410 MPa, 18.5% and 114 HV from 230 MPa, and 5.1% and 80 HV, respectively. Thus, WE43 microtubes with high strength and ductility fabricated using the combined approach can be used as BVS [25].

The Mg-Zn-Y-Nd alloy has become one of the most promising Mg vascular stent materials. The Mg-Zn-Y-Nd alloy with high mechanical properties and good corrosion resistance was investigated by Wang et al. [19]. High precision Mg-Zn-Y-Nd microtubes with an outer diameter of 2 mm and wall thickness of 0.15 mm were fabricated by HE, multipass CD, and interpass annealing. The UTS and elongation were 298 MPa and 20%, respectively. The alloy exhibited good corrosion resistance with a trend of uniform corrosion in a simulated body fluid solution.

The Mg alloys achieved relatively high mechanical properties satisfying the vascular stent requirements by alloying and advanced processing or a combination of both. Additional recent studies on Mg microtube manufacturing are listed in Table 2.

Novel Mg alloys with relatively high mechanical properties satisfying the BVS requirements have been investigated by the author. The Mg-4Zn-1Y alloy, which was designed based on the formation of the quasicrystal phase of the I-Phase (Mg_3Zn_6Y) to achieve high mechanical properties, was investigated by the author (Table 2). The Mg-4Zn-1Y alloy was fabricated using HE followed by ageing treatment. The YS, UTS, and elongation of the peaking-aged alloy were 240.7 MPa, 330.3 MPa, and 20.4%, respectively. The peaking-aged alloy was strengthened by the grain refinement, distortion, and precipitation of the I-Phase, which was an icosahedral quasicrystal structure with high hardness, high strength, and low surface energy. The Mg-4Zn-1Y alloy has great potential for use in vascular stents, but the corrosion behavior still requires clarification.

3.3. Degradation and Biocompatibility of Mg-Based Vascular Stents. Mg and its alloys degrade according to Equations (1)–(3). The hydrogen released during the process of Mg corrosion accelerates the corrosion rate, damages the coating, and forms gas cavities at the stents. Alloying and coating have been investigated for inhibiting the corrosion rate of magnesium alloys [33]:

$$\text{Anodic reaction}: \mathrm{Mg} \rightarrow \mathrm{Mg^{2+}} + 2\mathrm{e^-} \quad (1)$$

$$\text{Cathodic reaction}: 2\mathrm{H_2O} + 2\mathrm{e^-} \rightarrow \mathrm{H_2} + 2\mathrm{OH^-} \quad (2)$$

$$\mathrm{Mg(OH)_2}\ \text{formation}: 2\mathrm{Mg^{2+}} + 2\mathrm{OH^-} \rightarrow \mathrm{Mg(OH)_2} \quad (3)$$

To reduce the corrosion rate and improve the biological response, surface modification methods including plasma,

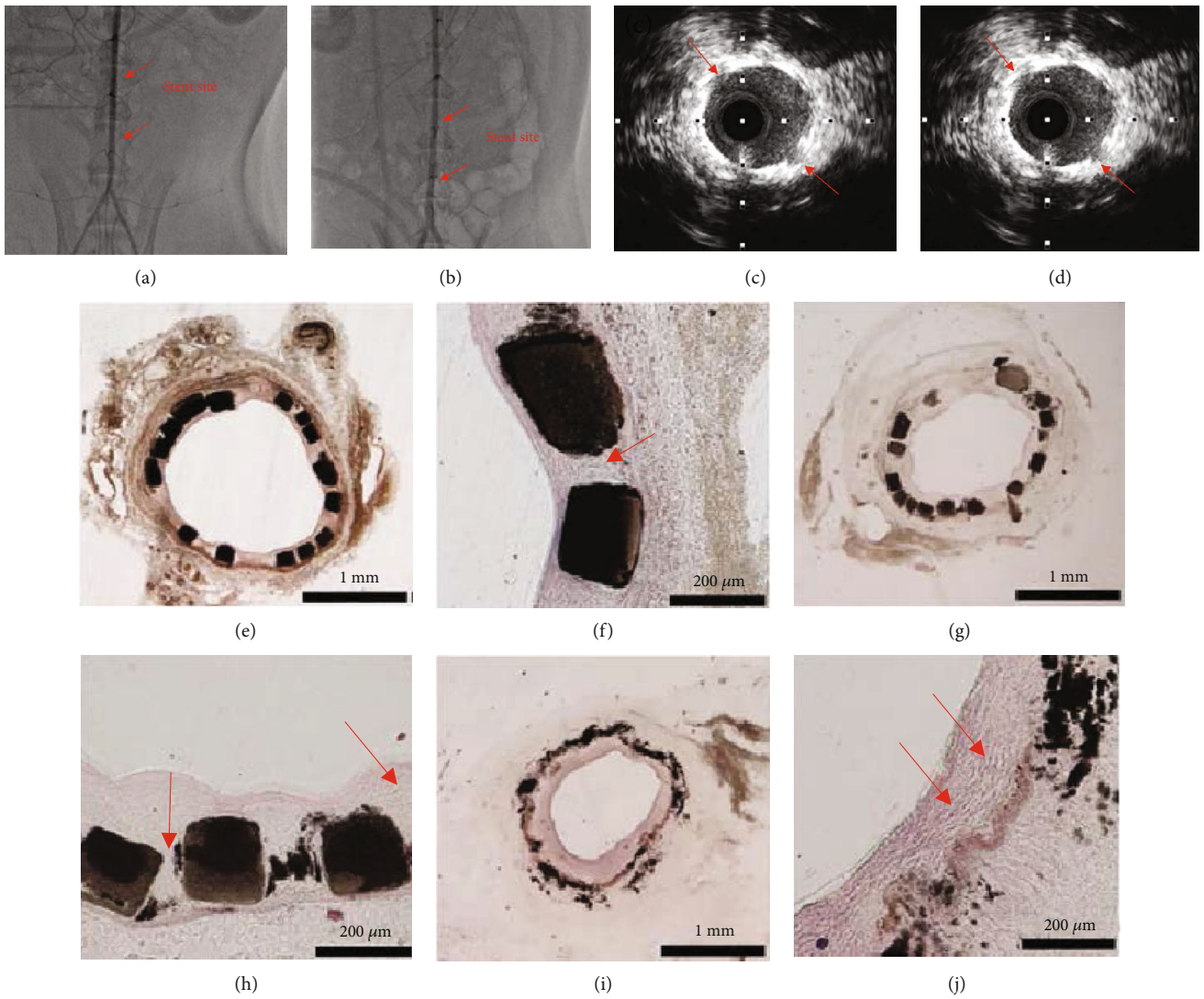

Figure 4: Angiographic and intravascular ultrasound images of implantation for 28 days in abdominal aorta with JDBM and MgF2-coated JDBM [34, 37]: (a, c) JDBM; (b, d) MgF2-coated JDBM. Histological examination results of implanting JDBM stents for 1, 4, and 12 months: (e, f) 1 month; (g, h) 4 months; (i, j) 12 months.

ion irradiation, and coatings have been employed in combination with alloying and microstructure refinement. The coatings include PLGA, MgF_2, PEUU, and PCUU. A nanoscale MgF_2 film was developed on a Mg-2.5Nd-0.2Zn-0.4Zr (JDBM) alloy by Mao et al. [34]. The corrosion rate protected by a nanoscale MgF_2 film with a uniform and dense structure decreased from 0.337 to 0.269 mm/year. An animal experiment, wherein a MgF_2-coated JDBM alloy stent was implanted to the abdominal aorta of a rabbit, was conducted to investigate the biosafety and efficacy (Figures 4(a)–4(d)). The angiography images indicated that thrombosis or restenosis did not occur for neither the naked nor the coated stents (Figures 4(a) and 4(b)), and the intravascular ultrasound images revealed that strut fracture or restenosis did not occur (Figures 4(c) and 4(d)). The results revealed that the adequately reendothelialized stent had excellent tissue compatibility without thrombogenesis and restenosis in the test vessel.

The *in vitro* and *in vivo* investigation of the degradation behavior of the rapamycin-eluting JDBM alloy was investigated by Shi et al. [35]. The results revealed that the polymeric coating protected the alloy against degradation both in the short term and in the long term. A remarkably lower degradation rate was observed in a micro-CT test, and the radical supporting *in vivo* duration of the drug-eluting JDBM stent was prolonged compared with that of the bare stent. The rapamycin-eluting JDBM alloy exhibited great potential for use as a BVS.

To further investigate the safety, efficacy, and degradation behavior of the JDBM alloy, a 20-month observation was conducted by Zhang et al. after a stent had been implanted into the common carotid artery of a New Zealand white rabbit [36]. The results revealed that the implanted JDBM stent had good safety with complete reendothelialization in 28 days, and the struts were replaced in situ by degradation products within four months. The histological examination images of implanting for 1, 4, and 12 months are shown in Figures 4(e)–4(j). The struts were completely embedded by intima in one month (Figures 4(e) and 4(f)),

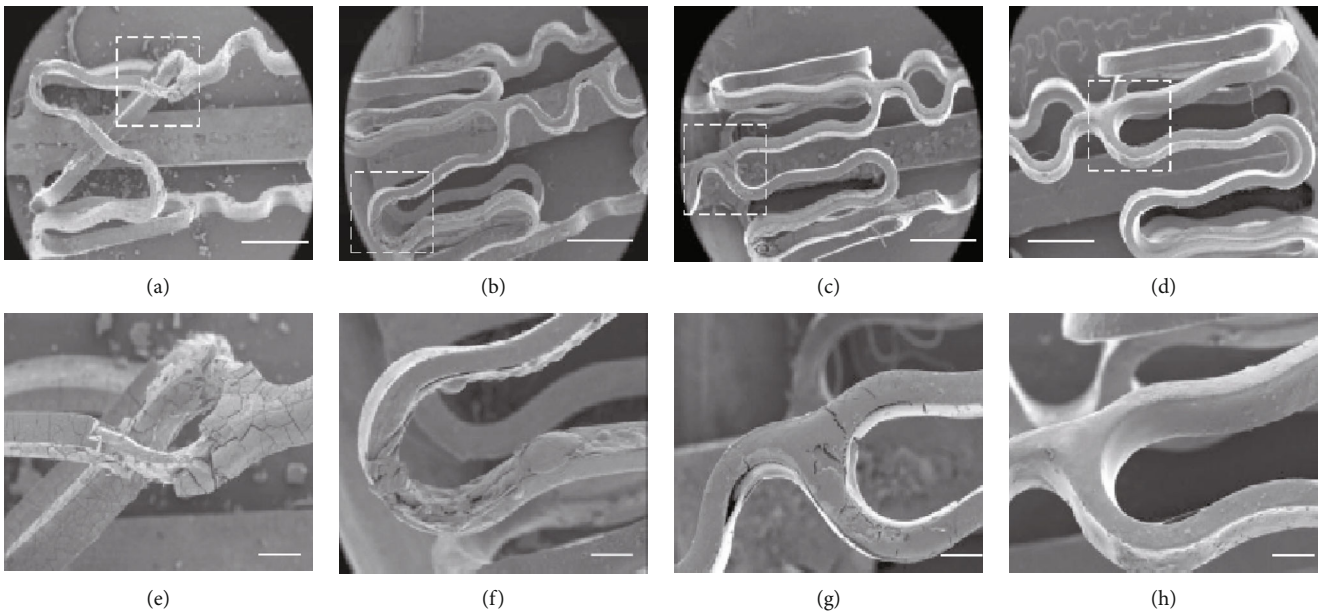

Figure 5: SEM images of corrosion regions on AZ31 stents [37]: (a, e) noncoated; (b, f) PLGA; (c, g) PEUU; (d, h) PCUU; scale bar = 1 mm: top row; 200 μm: bottom row.

and degradation products with irregular shapes appeared after four months (Figures 4(g) and 4(h)). After 12 months, the stent completely degraded into scattered fragments (Figures 4(i) and 4(j)). The Ca concentration of the degradation products decreased in the long term, and thus, vessel calcification was avoided. The Mg and Zn elements were metabolized, while the Nd and Zr elements remarkably increased in the spleen and liver within one month.

Poly(carbonate urethane) urea (PCUU), poly(ester urethane) urea (PEUU), and poly(lactic-co-glycolic acid) (PLGA) are also mainly used for coating Mg stents. The dynamic degradation behaviors, hemocompatibility, and drug release were investigated for three different coated AZ31 stents by Gu et al. [37] The SEM morphology of one noncoated and three coated AZ31 alloy stents in the perfusion bioreactor under a wall shear stress of 0.07 Pa for three days in DMEM (10% FBS, 1% P/S) mixed with 100 U/mL lipase solution is shown in Figure 5 [37]. Owing to the decreased tensile properties caused by degradation, various noncoated stent struts were distorted (Figures 5(a) and 5(e)). Blebbing was observed across the PLGA-coated stent (Figures 5(b) and 5(f)), and various cracks were observed on the surface of the PEUU-coated stent (Figures 5(c) and 5(g)). For the PCUU-coated stent, a generally smooth and intact surface was observed (Figures 5(d) and 5(h)).

Fast degradation is a limitation of Mg alloys used as biodegradable vascular stents, and focus has been directed toward improving the corrosion rate of Mg alloys. Recent studies on surface modification for improving the degradation of Mg-based vascular stents are briefly summarized in Table 3.

AZ31 alloy-based Mg vascular stents have also been preliminarily investigated by the author. An AZ31 sheet with a thickness of 250 μm was produced by photochemical etching; then, the Mg sheet with two small bands was laser-welded. AZ31 stents coated with polyhexymethylene carbonate urethane urea (PCUU) were investigated and exhibited great corrosion resistance under a flow-induced solution. Microcavities were laser-engraved to make the stents multifunctional, including functions such as drug storage and eluting. Plasma processing was employed to decrease the contact angle such that the liquid drug can better dissolve into the microcavities. The results revealed that the plasma processing was adequately effective in decreasing the contact angle between the Mg stents and the liquid drug. The AZ31 alloy has great potential for wide use as a vascular stent, but shape design, mechanical properties, drug eluting, corrosion protection, and *in vivo* experiments are still required for improving the material and stents.

4. Zn Alloys for Biodegradable Vascular Stents

Zn-based alloys with relatively high corrosion resistance are being considered for use as BVS owing to the tissue compatibility of iron and relatively fast degradation rate of Mg alloys. On one hand, the recommended value of the Zn element for biological functions is 10 mg/day. Additionally, according to Vojtech et al., the Zn element produced by the degradation of the Zn alloy is almost negligible compared with the daily limit of 10 mg [43]. The Zn element is required to support protein metabolism, cell growth, division, and so on. Thus, the degradation can be integrated into the daily activity of the human body, and toxic by-products can be avoided [44]. On the other hand, Zn alloys have a moderate degradation rate, which is faster than that of iron but slower than that of Mg alloys, owing to the protection of the corrosion production. Finally, Zn alloy stents are easier to manufacture owing to this material's low melting point, low chemical reactivity, and excellent machinability. Moreover, Zn alloys can be casted under an air atmosphere, while Mg alloys must be

Table 3: Recent studies on degradation of Mg alloys.

Alloy	Surface modification	Corrosion and compatibility tests	Results
JDBM [34]	Nanoscale MgF_2 film coating.	Artificial plasma; 2.5-3.5 kg, sex-unlimited, 3-4-month-old, healthy, clean New Zealand white rabbits.	The corrosion rate of coated JDBM exposed to artificial plasma was reduced from 0.377 ± 0.021 to 0.269 ± 0.043 mm/year. Excellent tissue compatibility of adequately reendothelialized stent with no sign of thrombogenesis and restenosis in the stent-supported vessel.
AZ31 [37]	PCUU; PLGA; PEUU coatings.	Dulbecco's modified Eagle's medium (DMEM) supplemented with 10% fetal bovine serum (FBS), 1% penicillin/streptomycin (P/S), and 100 U/mL lipase solution; whole ovine blood for blood contacting test.	The PCUU-coated Mg stents exhibited improved corrosion resistance compared with the uncoated and PLGA-coated stents; the PCUU-coated Mg stents exhibited reduced thrombotic deposition versus the uncoated and PLGA-coated stents; the release of paclitaxel from the PCUU coating effectively inhibited rSMC proliferation.
AZ31 [38]	The first and third layers were low molecular weight dextran loaded with sirolimus, and the second layer was PGA.	DC polarization and immersion tests; culturing cells for indirect cell viability and cell proliferation tests; hemolysis assay for blood compatibility.	Coating increased the corrosion resistance, cell viability, and proliferation rate and was nonhemolytic; the released sirolimus had no obvious effect on cell viability but could inhibit cell proliferation.
WE43 [39]	3.6 μg/mm paclitaxel by ultrasonic modification.	Iliac artery of New Zealand white rabbits with weight of 2.5-3.0 kg.	The corrosion rate was fast in PBS, deployment was safe, and endothelial coverage occurred after 42 days; the corrosion rate needs to be slower or the mechanical properties require improvement to scaffold the arteries for 183 days.
Mg-Zn-Y-Nd [40]	Lower layer: MgF2; upper layer: polydopamine.	Immersion test and electrochemical test.	Coated Mg stents exhibited a dramatic corrosion rate improvement in electrochemical and immersion degradation tests for 14 days; coating created favorable environment for ECs to have competitive advantage over vascular smooth muscle cells.
Mg-Zn-Y-Nd [41]	AA-PEUU; Arg-Leu-PEUUs.	Long-term immersion and electrochemical tests by standard Hank's solution (pH = 7.4 at 37°C); HUVEC and HASMC for *in vitro* cytocompatibility.	Arg-Leu-PEUU-coated Mg-Zn-Y-Nd alloys improved corrosion resistance, reduced hemolysis rate and platelet adhesion, and exhibited better cytocompatibility with better cellular morphology, proliferation, and biofunctionality in *in vitro* experiment.
Mg-Zn-Y-Zn [42]	BTSE; APTES; PLGA.	Electrochemical measurements and long-term immersion tests; VSMC and HUVEC for cell adhesion and cell viability tests.	The anticorrosion capacity was greatly enhanced by coating; pre-treated PLGA coating as modified PLGA coating was effective in improving the corrosion behavior and biocompatibility.

*PCUU: poly(carbonate urethane) urea; PEUU: poly(ester urethane) urea; PLGA: poly(lactic-co-glycolic acid); AA-PEUU: amino acid-based poly(ester urea urethane); PGA: polyglutamic acid; Arg-Leu-PEUUs: arginine-leucine-based poly(ester urea urethane); BTSE: bistriethoxysilylethane; APTES: amino-propyltrimethoxysilane; HUVEC: human umbilical vein endothelial cell line; HASMC: human aortic vascular smooth muscle primary cell; VSMC: vascular smooth muscle cells.

processed with protection against N_2 and SF_6, which are harmful to human health [45].

4.1. Processes and Mechanical Properties of Zn Microtubes. The process of fabricating Zn-based BVS is similar to the process of fabricating Mg-alloy-based BVS. Moreover, Zn alloys are HCP structures and thus deform with great difficulty. Therefore, the improvement of the mechanical properties of Zn alloys, which is the biggest limitation to their use as BVS, is very important.

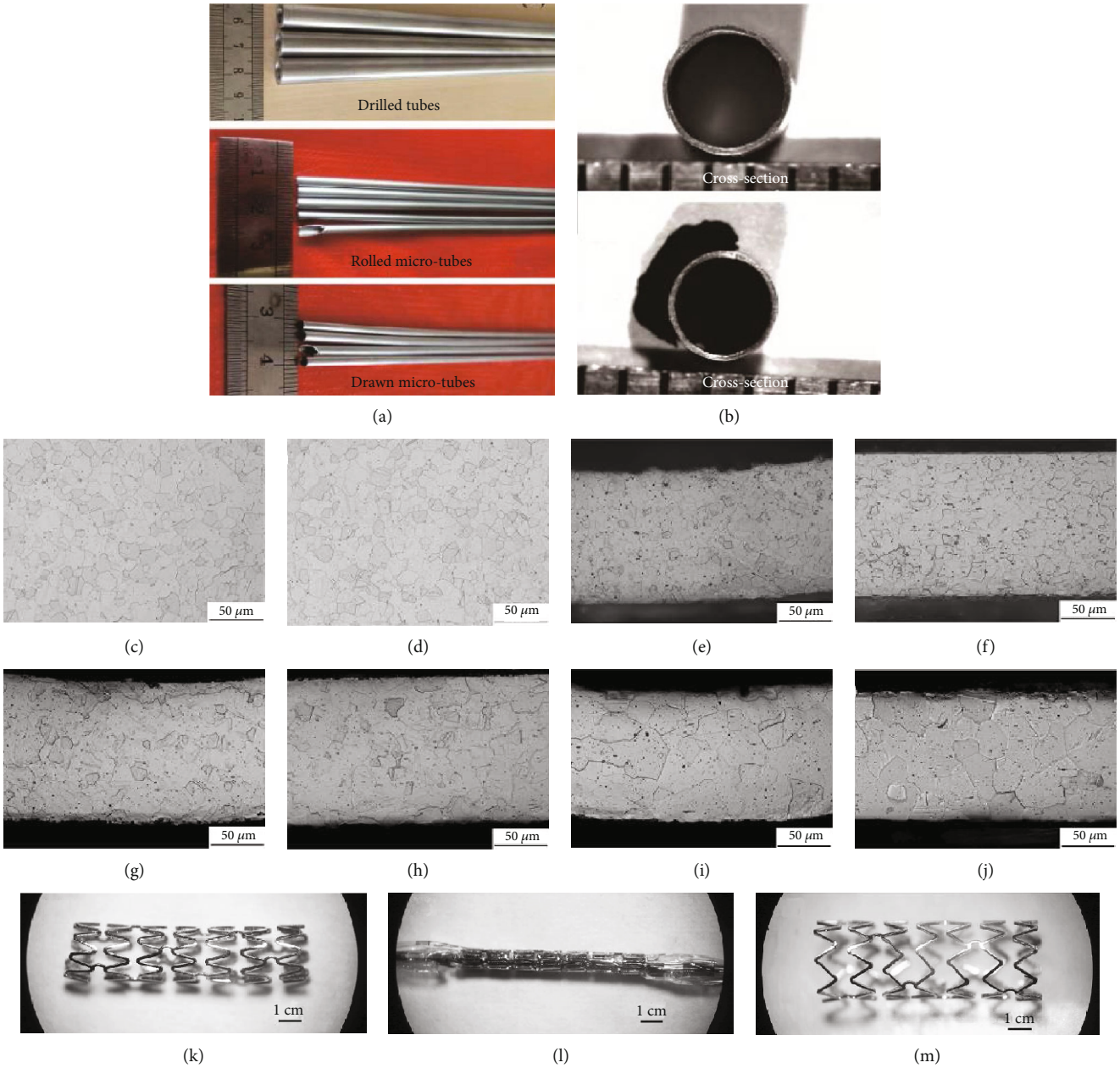

Figure 6: Microtube of Zn-0.05Mg-0.01Fe alloy fabricated by drilling, rolling, and drawing [44]: (a) microtube; (b) cross-section of microtube. Microstructure of Zn microtubes: drilling, (c) cross-section and (d) longitudinal section; rolling, (e) cross-section and (f) longitudinal section; drawing, (g) cross-section and (h) longitudinal section; annealing, (i) cross-section and (j) longitudinal section. Zn-based vascular stents fabricated by laser etching and electrochemical polishing: (k) Zn-based stent with diameter of 2.5 mm; (l) first crimp to diameter of 1.3 mm; (m) balloon expansion to diameter of 3.5 mm.

Zn-0.05Mg-0.01Fe microtubes were fabricated by Wang et al. using drilling, rolling, and drawing [44]. The microtubes with an outer diameter of 2.5 mm and thickness of 130 μm (Figures 6(a) and 2(b)) exhibited an UTS of 220 MPa. The microstructures of the drilling, rolling, cold drawing, and annealing microtubes are shown in Figures 6(c)–6(j). Both the drilling and rolling microtubes exhibited a homogeneous microstructure (Figures 6(c)–6(f)), and twinning occurred after cold drawing, which assisted the HCP structure of Zn alloys in achieving larger plastic deformation (Figures 6(g) and 6(h)). Subsequently, DRX grains were observed after annealing with an average grain size of 20 μm (Figures 6(i) and 6(j)). The microtubes were fabricated into stents by laser etching and electrochemical polishing, as shown in Figure 6(k). Additionally, microcracks were not observed when the stent crimped to a diameter of 1.3 mm (Figure 6(l)), and the balloon expanded to a diameter of 3.5 mm (Figure 6(m)). Thus, the microtubes exhibited better expansion properties compared with stents with welding bars.

The Zn-4Cu alloy was fabricated by Niu et al. using hot extrusion [46]. The YS, UTS, and elongation of the extruded alloy were 250 MPa, 270 MPa, and 51%, respectively, owing

Table 4: Recently reported processing and properties of wrought Zn alloys.

Alloys	Processes	Dimensions	YS (MPa)	UTS (MPa)	EL (%)
Zn-0.15Mg [48]	DE+TE	Tube: outer diameter of 4 mm; inner diameter of 1.5 mm	114	250	22
Zn-0.5Mg [48]			159	297	13
Zn-1Mg [48]			180	340	6
Zn-3Mg [48]			291	399	1
Zn-1Mg-1Ca [49]	HR HE	—	210	260	5.5
Zn-1Mg-1Sr [49]			200	250	7.5
Zn-1Ca-1Sr [49]			215	265	6.8
Zn-1Mg-0.1Sr [50]	HR	Sheet metal: thickness of 2.1	196	300	22.49
Zn-1Mg-0.1Mn [51]		Sheet metal: thickness of 2.1	195	299	26.07
Zn-1Ca [52]	HE	Rod: diameter of 10 mm	195	240	7.5
Zn-1Sr [52]			220	260	10.8
Zn-1Mg [52]			205	265	8.5
Zn-0.5Al [48]	DE+TE	Tube: outer diameter of 4 mm; inner diameter of 1.5 mm	119	203	33
Zn-1Al [48]			134	223	24
Zn-1Cu [15]	HE	Rod: diameter of 20 mm	149	186	21
Zn-2Cu [15]			199	240	46.8
Zn-3Cu [15]			213	257	47.2
Zn-4Cu [15]			227	270	50.6
Zn-3Cu-0.1Mg [53]	HE	Rod: diameter of 20 mm	340	375	5
Zn-3Cu-0.5Mg [53]			400	425	2
Zn-3Cu-1Mg [53]			425	450	1
Zn-2.5Ag [54]	HE	Rod: extrusion ratio of 14 : 1	155	205	35
Zn-5.0Ag [54]			210	260	38
Zn-7.0Ag [54]			240	290	32

*DE: direct extrusion; TE: tube extrusion; HE: hot extrusion; HR: hot rolling.

to the distribution of the strengthening phase of the $CuZn_5$ and DRX. The *in vitro* evaluation revealed that the corrosion rate of the Zn-4Cu was approximately 9.41 μm/year, and corrosion products with acceptable toxicity were released.

The Zn-0.1Li alloy was vacuum casted, then extruded, and finally drawn into wires with a diameter of 0.25 mm by Zhao et al. [47]. The UTS of pure Zn increased from 116 MPa to 274 MPa, while the elongation remained at 17%. From the longitudinal section microstructure, an orientation with an angle of 27° to the extrusion direction was observed and may have been generated from the non-basal <c+a> slip system. From the cross-section, a eutectic microstructure was observed with bright matrix phases and dark phases of the Li-rich precipitates with an average grain size of 3 μm.

Zn-0.002Mg, Zn-0.005Mg, and Zn-0.08Mg wires with a diameter of 0.25 mm were evaluated as potential biodegradable materials and fabricated by Jin et al., who used casting, extrusion, and drawing [14]. Zn-0.08Mg exhibited the greatest mechanical properties with a YS, UTS, and elongation of 200-300 MPa, 300-400 MPa, and 40%, respectively. However, the Zn-0.08Mg alloy exhibited strain rate sensitivity and strain softening after yield, both of which must be addressed before this alloy can be used as a BVS material.

The processing of Zn-based microtubes is very limited compared with that of Mg alloys. Recent studies on wrought Zn alloys for biomedical applications are summarized in Table 4.

4.2. Degradation and Biocompatibility of Zn-Based Stents. The corrosion of Zn alloys is expressed by Equations (4)–(7). Gas is not released during the corrosion process. During the corrosion period, three layers are formed: calcium/phosphorus, zinc oxide, and zinc carbonate. Additionally, the degradation products are similar to those of Mg alloys.

$$\text{Anodic reaction}: 2Zn \rightarrow 2Zn^{2+} + 4e^{-} \quad (4)$$

$$\text{Cathodic reaction}: O_2 + 2H_2O + 4e^{-} \rightarrow 4OH^{-} \quad (5)$$

$$Zn(OH)_2 \text{ formation}: 2Zn^{2+} + 4OH^{-} \rightarrow 2Zn(OH)_2 \quad (6)$$

$$\text{ZnO formation}: Zn(OH)_2 \rightarrow ZnO + H_2O \quad (7)$$

For the Zn-0.1Li alloy discussed in Section 4.1 [47], the *in vivo* corrosion behavior and biocompatibility were also investigated. The results obtained by the corrosion experiments for implantation from 2 to 12 months revealed that the degradation rate was 0.008 to 0.016 mm/year after 2 to 4 months and increased to 0.019 mm/year and 0.046 mm/year after 9 and 12 months, respectively. The images obtained by the *in vivo* biocompatibility analysis are shown in Figures 7(a)–7(c).

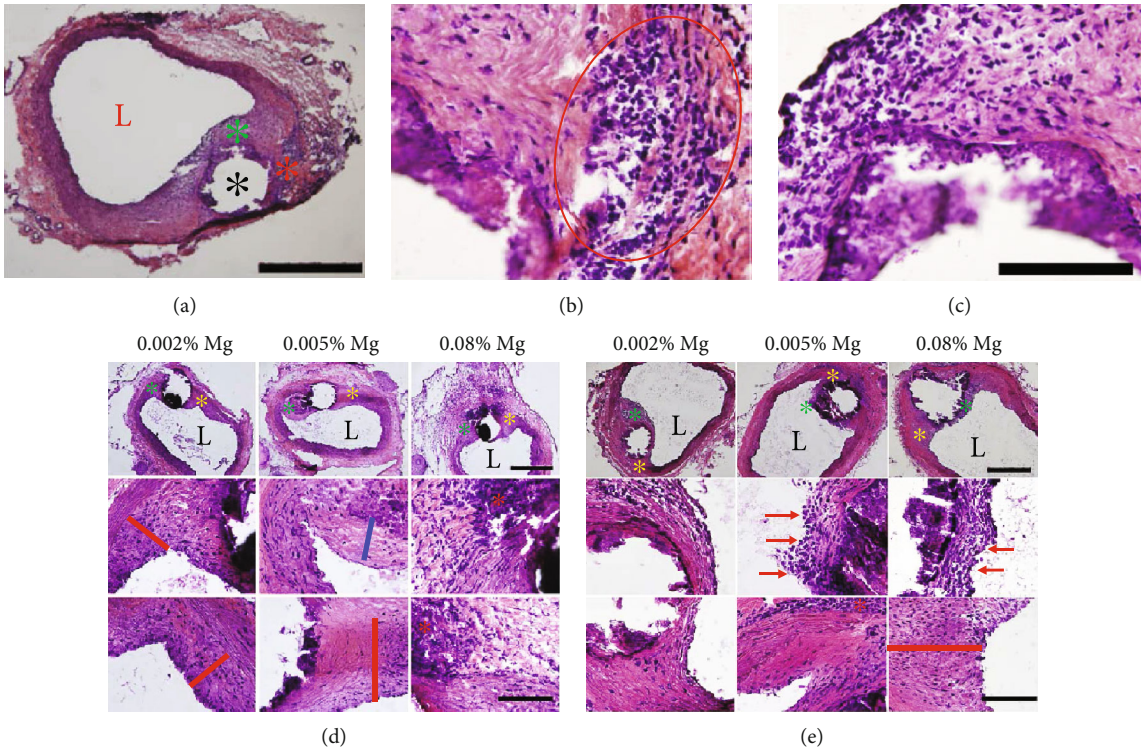

Figure 7: Arterial explants stained with H&E at 11 months [14]. The black asterisk in (a) indicates the wire location with a scale of 500 μm; (b, c) scale of 100 μm [47]. (d, e) Histological examination results for implanting Zn-xMg (x = 0.002, 0.005, and 0.08) stents for 6 and 11 months.

Table 5: In vitro studies on the cytotoxicity of Zn and its alloys.

Alloy	Cell and culture	Results
Pure zinc [55]	(1) Human dermal fibroblasts (hDF) for representing adventitial tissue. (2) Human aortic smooth muscle cells (AoSMC) for mimicking tunica media. (3) Human aortic endothelial cells (HAEC) as replacement for tunica intima.	The LD50 values for hDf, AoSMC, and HAEC were 50 μm, 70 μm, and 265 μm, respectively. Cell attachment, spreading, and migration were affected by increased Zn levels.
Pure zinc [56]	Human mesenchymal stem cell (hMSC) derived from bone marrow. Culture medium was α-MEM without nucleotides, containing 10% FBS and 1% penicillin/streptomycin.	Cell motility was higher for Zn than for AZ31. The mineralization of ECM and hMSC osteogenic differentiation was enhanced when cells were cultured with Zn or AZ31 with increased expression of bone-related genes, including ALP, collagen I, and osteopontin. The intracellular Zn^{2+} led to the enhanced regulation of genes, cell survival/growth and differentiation, ECM mineralization, and osteogenesis.
Zn-0.8Mg [57] Zn-1.6Mg	U-2 OS cells (human cell line derived from osteosarcoma) maintained in Dulbecco's modified Eagle's medium; L929 cells (murine fibroblasts) maintained in minimum essential medium.	Zn is less biocompatible than Mg, and the maximum safe concentration of Zn^{2+} for U-2 OS and L929 cells is 120 μM and 80 μM, respectively. Genotoxicity and mutagenicity tests did not indicate any negative effect connected with the use of Zn.
Zn-1.5Mg [58]	U-2 OS cells (human cell line derived from osteosarcoma); L929 cells (murine fibroblasts).	Preincubation decreased the initial corrosion rate of the alloy and increased the metabolic activity of L929 after indirect testing and number of U-2 OS cells adhering onto the alloy surface. The osteoblast-like cell grew directly on the samples.
Zn-xCu [15] (x = 1, 2, 3, 4)	Human endothelium cell line (EA. Hy926).	Zn-Cu alloys are cytocompatible to human endothelial cells; the antibacterial property is ideal when the Cu concentration is higher than 2% in weight.

The open arterial lumens and low neointimal growth indicate the excellent biocompatibility of the Zn-Li alloy.

For the Zn-0.002Mg, Zn-0.005Mg, and Zn-0.08Mg wires discussed in Section 4.1 [14], slightly elevated inflammation and neointimal activation were observed in the degradation tests in the abdominal aorta of adult male Sprague-Dawley rats for 1.5, 3, 4.5, 6, and 11 months. The histological examination results for implantation for 6 and 11 months are shown in Figures 7(d) and 7(e), respectively. The results revealed that inflammation was caused by the implantation, but the inflammation caused by the Zn-0.08Mg alloy subsided after 6 to 11 months. The Zn-0.08Mg alloy can potentially be used as a BVS, but the mechanical properties, which were sufficient under various loading conditions, require further investigation to eliminate the strain rate sensitivity.

There only exists a small number of *in vitro* studies on the cytotoxicity of Zn alloys. These studies are briefly summarized in Table 5.

5. Conclusions and Perspectives

Biodegradable Mg alloys are being widely investigated for implantation applications such as vascular stents. Relatively low mechanical properties and an effective working lifetime are required by the implantation applications. Mg alloys, which are the primary metallic materials with good biodegradability, can provide sufficiently high tensile properties to serve as BVS. However, their relatively fast corrosion rate requires additional coating to protect the Mg stents from body fluids at the early stages of implantation and degradation.

For the development of Mg-based biodegradable vascular stents, this review focused on the following considerations: (1) stent fabrication based on microtubes should be the main process for avoiding welding bars, which can increase the cost and cause nonuniform stress distribution; (2) despite microtubes being employed as the stent basis, the structure of stents should be better designed and modified through finite element analysis and *in vitro* experiments; (3) considering that numerous advanced fabrication processes have been developed and employed for microtube manufacturing, studies should focus on degradation and biocompatibility, including coating, surface modification, and multifunctional design, to solve the biggest inhibitors of Mg vascular stent applications; (4) biodegradable drug-eluting vascular stents should be at the forefront of relevant research.

Biodegradable Zn alloys have been much less investigated than Mg alloys. Preliminary investigation results have revealed that Zn alloys have much better corrosion resistance without gas release, compared with Mg alloys. This can be beneficial to the use of Zn alloys as BVS. Moreover, the preliminary investigation results revealed that Zn-based alloys used as vascular stents have a greater appropriate corrosion rate compared with iron-based and Mg-based stents. However, the limitation of the relatively low mechanical properties requires further investigation.

With regard to the development of Zn-based biodegradable vascular stents, the following conclusions can be drawn: (1) more alloying and advanced processing methods should be employed to develop Zn-based microtubes and improve their mechanical properties, which are the biggest limitation hindering their use in stent applications. Preliminary research results have revealed that extrusion and rolling are the only two methods for fabricating Zn rods but are poorly investigated, particularly with regard to microtube manufacturing. Thus, future work should focus on the fabrication of microtubes and stents by employing CCE or SPD, even if the brittleness of Zn is stronger than that of Mg alloys; (2) finite element analysis should be carried out for stent design and modification according to the specific properties of Zn alloys; (3) degradation and biocompatibility should be further investigated by conducting *in vivo* experiments and animal experiments to obtain data for Zn-based vascular stents.

Conflicts of Interest

The authors declare that there is no conflict of interest regarding the publication of this paper.

Acknowledgments

This work was supported by the National Natural Science Foundation of China (Grant No. 81802413).

References

[1] Q. Feng, D. Zhang, C. Xin et al., "Characterization and in vivo evaluation of a bio-corrodible nitrided iron stent," *Journal of Materials Science. Materials in Medicine*, vol. 24, no. 3, pp. 713–724, 2013.

[2] J. E. Schaffer, E. A. Nauman, and L. A. Stanciu, "Cold drawn bioabsorbable ferrous and ferrous composite wires: an evaluation of in vitro vascular cytocompatibility," *Acta Biomaterialia*, vol. 9, no. 10, pp. 8574–8584, 2013.

[3] S. E. Hassani, W. W. Chu, R. M. Wolfram et al., "Clinical outcomes after percutaneous coronary intervention with drug-eluting stents in dialysis patients," *The Journal of Invasive Cardiology*, vol. 18, no. 6, pp. 273–277, 2006.

[4] Y. Onuma, J. Ormiston, and P. W. Serruys, "Bioresorbable scaffold technologies," *Circulation Journal*, vol. 75, no. 3, pp. 509–520, 2011.

[5] R. D. Alexy and D. S. Levi, "Materials and manufacturing technologies available for production of a pediatric bioabsorbable stent," *BioMed Research International*, vol. 2013, Article ID 137985, 2013.

[6] S. Bangalore, B. Toklu, N. Amoroso et al., "Bare metal stents, durable polymer drug eluting stents, and biodegradable polymer drug eluting stents for coronary artery disease: mixed treatment comparison meta-analysis," *BMJ*, vol. 437, article f6625, 2016.

[7] T. M. Bedair, I. J. Min, W. Park, Y. K. Joung, and D. K. Han, "Sustained drug release using cobalt oxide nanowires for the preparation of polymer-free drug-eluting stents," *Journal of Biomaterials Applications*, vol. 33, no. 3, pp. 352–362, 2018.

[8] T. S. Jang, K. H. Cheon, J. H. Ahn, E. H. Song, H. E. Kim, and H. D. Jung, "In-vitro blood and vascular compatibility of sirolimus-eluting organic/inorganic hybrid stent coatings," *Colloids and Surfaces B: Biointerfaces*, vol. 179, pp. 405–413, 2019.

[9] S. Goel, R. T. Pasam, S. Chava et al., "Three to four years outcomes of the absorb bioresorbable vascular scaffold versus second-generation drug-eluting stent: A meta-analysis," *Catheterization and Cardiovascular Interventions*, 2019.

[10] T. Hu, C. Yang, S. Lin, Q. Yu, and G. Wang, "Biodegradable stents for coronary artery disease treatment: recent advances and future perspectives," *Materials Science & Engineering. C, Materials for Biological Applications*, vol. 91, pp. 163–178, 2018.

[11] E. Mostaed, M. Sikora-Jasinska, J. W. Drelich, and M. Vedani, "Zinc-based alloys for degradable vascular stent applications," *Acta Biomaterialia*, vol. 71, pp. 1–23, 2018.

[12] Q. de Hemptinne, F. Picard, R. Briki et al., "Drug-eluting resorbable magnesium scaffold implantation in ST-segment elevation myocardial infarction: a pilot study," *The Journal of Invasive Cardiology*, vol. 30, no. 6, pp. 202–206, 2018.

[13] D. Liu, S. Hu, X. Yin, J. Liu, Z. Jia, and Q. Li, "Degradation mechanism of magnesium alloy stent under simulated human micro- stress environment," *Materials Science & Engineering. C, Materials for Biological Applications*, vol. 84, pp. 263–270, 2018.

[14] H. Jin, S. Zhao, R. Guillory et al., "Novel high-strength, low-alloys Zn-Mg (<0.1wt% Mg) and their arterial biodegradation," *Materials Science & Engineering. C, Materials for Biological Applications*, vol. 84, pp. 67–79, 2018.

[15] Z. Tang, J. Niu, H. Huang et al., "Potential biodegradable Zn-Cu binary alloys developed for cardiovascular implant applications," *Journal of the Mechanical Behavior of Biomedical Materials*, vol. 72, pp. 182–191, 2017.

[16] P. K. Bowen, E. R. Shearier, S. Zhao et al., "Biodegradable Metals for Cardiovascular Stents: from Clinical Concerns to Recent Zn-Alloys," *Advanced Healthcare Materials*, vol. 5, no. 10, pp. 1121–1140, 2016.

[17] R. J. Werkhoven, W. H. Sillekens, and J. B. J. M. van Lieshout, "Processing aspects of magnesium alloy stent tube," in *Magnesium Technology 2011*, W. H. Sillekens, S. R. Agnew, N. R. Neelameggham, and S. N. Mathaudhu, Eds., pp. 419–424, Springer International Publishing, Champions, 2011.

[18] J. S. Lee, P. Han, E. Song et al., "Magnetically coated bioabsorbable stents for renormalization of arterial vessel walls after stent implantation," *Nano Letters*, vol. 18, no. 1, pp. 272–281, 2018.

[19] J. Wang, Y. Zhou, Z. Yang, S. Zhu, L. Wang, and S. Guan, "Processing and properties of magnesium alloy micro-tubes for biodegradable vascular stents," *Materials Science & Engineering. C, Materials for Biological Applications*, vol. 90, pp. 504–513, 2018.

[20] G. Li, N. Wang, X. Li et al., "Balloon-Mounted versus Self-Expanding Stent Outcomes in Symptomatic Middle Cerebral Artery Stenosis Combined with Poor Collaterals in China: A Multicenter Registry Study," *World Neurosurgery*, vol. 124, pp. e675–e681, 2019.

[21] S. A. Luffy, J. Wu, P. N. Kumta, and T. W. Gilbert, "Evaluation of magnesium alloys for use as an intraluminal tracheal for pediatric applications in a rat tracheal bypass model," *Journal of Biomedical Materials Research Part B: Applied Biomaterials*, vol. 107, no. 6, pp. 1844–1853, 2018.

[22] S. Amani and G. Faraji, "Processing and properties of biodegradable magnesium microtubes for using as vascular stents: a brief review," *Metals and Materials International*, vol. 25, no. 5, pp. 1341–1359, 2019.

[23] P. K. Bowen, J. Drelich, and J. Goldman, "Zinc exhibits ideal physiological corrosion behavior for bioabsorbable stents," *Advanced Materials*, vol. 25, no. 18, pp. 2577–2582, 2013.

[24] F. Liu, C. Chen, J. Niu et al., "The processing of Mg alloy micro-tubes for biodegradable vascular stents," *Materials Science & Engineering. C, Materials for Biological Applications*, vol. 48, pp. 400–407, 2015.

[25] S. Amani, G. Faraji, H. Kazemi Mehrabadi, K. Abrinia, and H. Ghanbari, "A combined method for producing high strength and ductility magnesium microtubes for biodegradable vascular stents application," *Journal of Alloys and Compounds*, vol. 723, pp. 467–476, 2017.

[26] T. Furushima and K.-i. Manabe, "Large reduction die-less mandrel drawing of magnesium alloy micro-tubes," *CIRP Annals*, vol. 67, no. 1, pp. 309–312, 2018.

[27] W. Lu, R. Yue, H. Miao, J. Pei, H. Huang, and G. Yuan, "Enhanced plasticity of magnesium alloy micro-tubes for vascular stents by double extrusion with large plastic deformation," *Materials Letters*, vol. 245, pp. 155–157, 2019.

[28] S. Amani and G. Faraji, "Recrystallization and mechanical properties of WE43 magnesium alloy processed via cyclic expansion extrusion," *International Journal of Minerals, Metallurgy, and Materials*, vol. 25, no. 6, pp. 672–681, 2018.

[29] S. Amani, G. Faraji, H. K. Mehrabadi, and M. Baghani, "Manufacturing and mechanical characterization of Mg-4Y-2Nd-0.4Zr-0.25La magnesium microtubes by combined severe plastic deformation process for biodegradable vascular stents," *Proceedings of the Institution of Mechanical Engineers, Part B: Journal of Engineering Manufacture*, vol. 233, no. 4, pp. 1196–1205, 2018.

[30] L. Wang, G. Fang, L. Qian, S. Leeflang, J. Duszczyk, and J. Zhou, "Forming of magnesium alloy microtubes in the fabrication of biodegradable stents," *Progress in Natural Science: Materials International*, vol. 24, no. 5, pp. 500–506, 2014.

[31] G. Fang, W. J. Ai, S. Leeflang, J. Duszczyk, and J. Zhou, "Multipass cold drawing of magnesium alloy minitubes for biodegradable vascular stents," *Materials Science & Engineering. C, Materials for Biological Applications*, vol. 33, no. 6, pp. 3481–3488, 2013.

[32] Q. Ge, D. Dellasega, A. G. Demir, and M. Vedani, "The processing of ultrafine-grained Mg tubes for biodegradable stents," *Acta Biomaterialia*, vol. 9, no. 10, pp. 8604–8610, 2013.

[33] D. Persaud-Sharma and A. McGoron, "Biodegradable magnesium alloys: a review of material development and *Applications*," *Journal of Biomimetics, Biomaterials and Tissue Engineering*, vol. 12, pp. 25–39, 2012.

[34] L. Mao, L. Shen, J. Chen et al., "Enhanced bioactivity of Mg–Nd–Zn–Zr alloy achieved with nanoscale MgF2 surface for vascular stent application," *ACS Applied Materials & Interfaces*, vol. 7, no. 9, pp. 5320–5330, 2015.

[35] Y. Shi, L. Zhang, J. Chen et al., "In vitro and in vivo degradation of rapamycin-eluting Mg-Nd-Zn-Zr alloy stents in porcine coronary arteries," *Materials Science & Engineering. C, Materials for Biological Applications*, vol. 80, pp. 1–6, 2017.

[36] J. Zhang, H. Li, W. Wang et al., "The degradation and transport mechanism of a Mg-Nd-Zn-Zr stent in rabbit common carotid artery: a 20-month study," *Acta Biomaterialia*, vol. 69, pp. 372–384, 2018.

[37] X. Gu, Z. Mao, S. H. Ye et al., "Biodegradable, elastomeric coatings with controlled anti-proliferative agent release for

magnesium-based cardiovascular stents," *Colloids and Surfaces. B, Biointerfaces*, vol. 144, pp. 170–179, 2016.

[38] J. Ma, N. Zhao, and D. Zhu, "Sirolimus-eluting dextran and polyglutamic acid hybrid coatings on AZ31 for stent applications," *Journal of Biomaterials Applications*, vol. 30, no. 5, pp. 579–588, 2015.

[39] C. L. Lu, H. Y. Dong, W. Wang, and G. Yang, "In Vivo and In Vitro studies of biodegradable WE43 stent," *Applied Mechanics and Materials*, vol. 528, pp. 70–76, 2014.

[40] X. Liu, Z. Zhen, J. Liu et al., "Multifunctional MgF2/polydopamine coating on Mg alloy for vascular stent application," *Journal of Materials Science & Technology*, vol. 31, no. 7, pp. 733–743, 2015.

[41] J. Liu, P. Wang, C. C. Chu, and T. Xi, "Arginine-leucine based poly (ester urea urethane) coating for Mg-Zn-Y-Nd alloy in cardiovascular stent applications," *Colloids and Surfaces. B, Biointerfaces*, vol. 159, pp. 78–88, 2017.

[42] J. Liu and T. Xi, "Enhanced anti-corrosion ability and biocompatibility of PLGA coatings on MgZnYNd alloy by BTSE-APTES pre-treatment for cardiovascular stent," *Journal of Materials Science & Technology*, vol. 32, no. 9, pp. 845–857, 2016.

[43] D. Vojtech, J. Kubasek, J. Serak, and P. Novak, "Mechanical and corrosion properties of newly developed biodegradable Zn-based alloys for bone fixation," *Acta Biomaterialia*, vol. 7, no. 9, pp. 3515–3522, 2011.

[44] C. Wang, Z. Yu, Y. Cui et al., "Processing of a novel Zn alloy micro-tube for biodegradable vascular stent application," *Journal of Materials Science & Technology*, vol. 32, no. 9, pp. 925–929, 2016.

[45] H. Ota, M. Mahmoudi, R. Torguson et al., "Safety and efficacy of everolimus-eluting stents for bare-metal in-stent restenosis," *Cardiovascular Revascularization Medicine*, vol. 16, no. 3, pp. 151–155, 2015.

[46] J. Niu, Z. Tang, H. Huang et al., "Research on a Zn-Cu alloy as a biodegradable material for potential vascular stents application," *Materials Science & Engineering. C, Materials for Biological Applications*, vol. 69, pp. 407–413, 2016.

[47] S. Zhao, J. M. Seitz, R. Eifler et al., "Zn-Li alloy after extrusion and drawing: structural, mechanical characterization, and biodegradation in abdominal aorta of rat," *Materials Science and Engineering: C*, vol. 76, pp. 301–312, 2017.

[48] E. Mostaed, M. Sikora-Jasinska, A. Mostaed et al., "Novel Zn-based alloys for biodegradable stent applications: design, development and in vitro degradation," *Journal of the Mechanical Behavior of Biomedical Materials*, vol. 60, pp. 581–602, 2016.

[49] H. Li, H. Yang, Y. Zheng, F. Zhou, K. Qiu, and X. Wang, "Design and characterizations of novel biodegradable ternary Zn-based alloys with IIA nutrient alloying elements Mg, Ca and Sr," *Materials & Design*, vol. 83, pp. 95–102, 2015.

[50] X. Liu, J. Sun, Y. Yang et al., "Microstructure, mechanical properties, in vitro degradation behavior and hemocompatibility of novel Zn-Mg-Sr alloys as biodegradable metals," *Materials Letters*, vol. 162, pp. 242–245, 2016.

[51] X. Liu, J. Sun, F. Zhou et al., "Micro-alloying with Mn in Zn-Mg alloy for future biodegradable metals application," *Materials & Design*, vol. 94, pp. 95–104, 2016.

[52] H. F. Li, X. H. Xie, Y. F. Zheng et al., "Development of biodegradable Zn-1X binary alloys with nutrient alloying elements Mg, Ca and Sr," *Scientific Reports*, vol. 5, no. 1, 2015.

[53] Z. Tang, H. Huang, J. Niu et al., "Design and characterizations of novel biodegradable Zn-Cu-Mg alloys for potential biodegradable implants," *Materials & Design*, vol. 117, pp. 84–94, 2017.

[54] M. Sikora-Jasinska, E. Mostaed, A. Mostaed, R. Beanland, D. Mantovani, and M. Vedani, "Fabrication, mechanical properties and in vitro degradation behavior of newly developed Zn–Ag alloys for degradable implant applications," *Materials Science & Engineering. C, Materials for Biological Applications*, vol. 77, pp. 1170–1181, 2017.

[55] E. R. Shearier, P. K. Bowen, W. He et al., "In vitro cytotoxicity, adhesion, and proliferation of human vascular cells exposed to zinc," *ACS Biomaterials Science & Engineering*, vol. 2, no. 4, pp. 634–642, 2016.

[56] D. Zhu, Y. Su, M. L. Young, J. Ma, Y. Zheng, and L. Tang, "Biological responses and mechanisms of human bone marrow mesenchymal stem cells to Zn and Mg biomaterials," *ACS Applied Materials & Interfaces*, vol. 9, no. 33, pp. 27453–27461, 2017.

[57] J. Kubásek, D. Vojtěch, E. Jablonská, I. Pospíšilová, J. Lipov, and T. Ruml, "Structure, mechanical characteristics and in vitro degradation, cytotoxicity, genotoxicity and mutagenicity of novel biodegradable Zn-Mg alloys," *Materials Science and Engineering: C*, vol. 58, pp. 24–35, 2016.

[58] E. Jablonska, D. Vojtech, M. Fousova et al., "Influence of surface pre-treatment on the cytocompatibility of a novel biodegradable ZnMg alloy," *Materials Science & Engineering. C, Materials for Biological Applications*, vol. 68, pp. 198–204, 2016.


The Scientific
World Journal
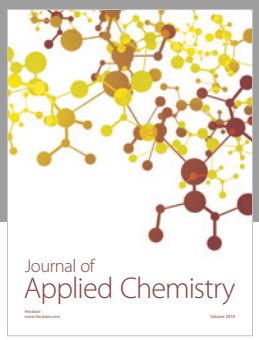
Journal of
Applied Chemistry
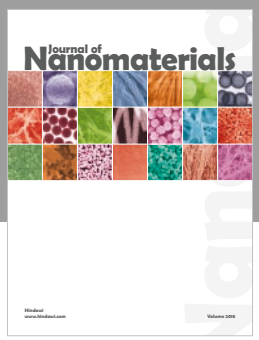
Journal of
Nanomaterials

Scientifica

International Journal of
Polymer Science
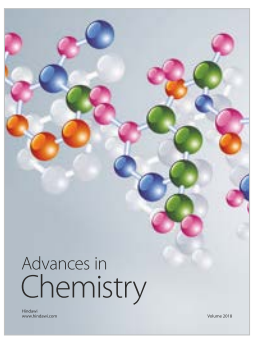
Advances in
Chemistry

Hindawi
Submit your manuscripts at
www.hindawi.com
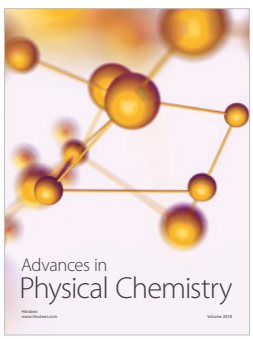
Advances in
Physical Chemistry

International Journal of
Analytical Chemistry
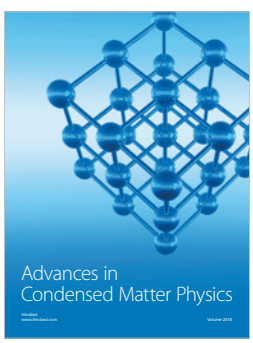
Advances in
Condensed Matter Physics
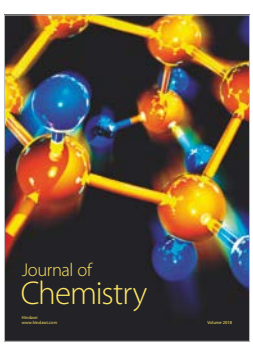
Journal of
Chemistry

International Journal of
Biomaterials
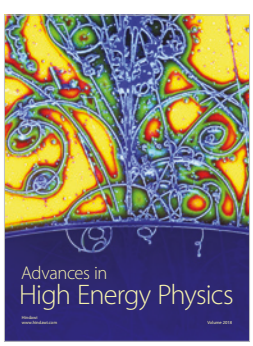
Advances in
High Energy Physics

Journal of
Engineering

Journal of
Nanotechnology

International Journal of
Corrosion

Journal of
Materials

BioMed
Research International
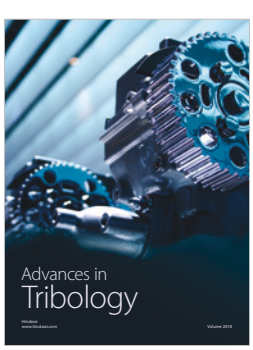
Advances in
Tribology
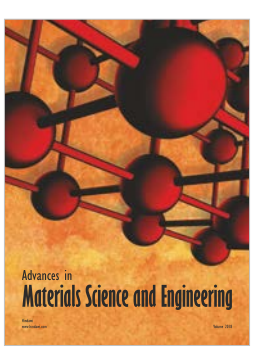
Advances in
Materials Science and Engineering